Identification of constitutive theory parameters using a tensile machine for deposited filaments of microcrystalline ink by Direct-Write Method

N. Lourdel, D. Therriault and M. Lévesque

Mechanical Engineering Department, Center for Applied Research on Polymers and Composites (CREPEC), École Polytechnique de Montréal, Montréal, Québec H3C 3A7, Canada

E-mail: martin.levesque@polymtl.ca

Abstract. A custom-designed tensile machine is developped to characterize the mechanical properties of ink micro-filaments deposited by Direct-Write method. The Direct-Write method has been used for the fabrication of a wide variety of micro-systems such as microvascular networks, chaotic mixers and laboratory on-chips. The tensile machine was used to measure the induced force in ink filaments during tensile and tension-relaxation tests as a function of the applied strain rate, the ink composition and the filament diameter. Experimental data was fitted by a linearly viscoelastic model using a data reduction procedure in order to identify the constitutive theory parameters of the deposited ink filaments. The model predictions based on the defined constitutive theory parameters were closed to the experimental data generated in this study. Such models will be useful in the development and optimization of future 3D complex structures made by direct-write method.

Submitted to: *J. Micromech. Microeng.*

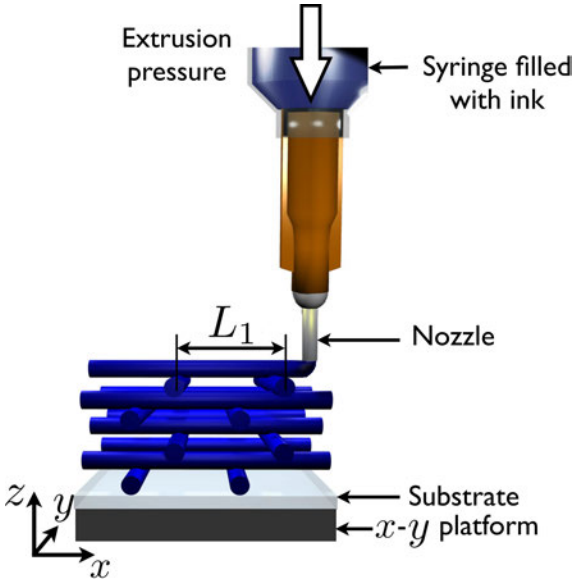

Figure 1. Schematic representation of a scaffold robotic deposition. Ink stored in a syringe is extruded through a nozzle under a constant pressure and deposited on a substrate in a defined pattern by adjusting the x-y platform displacements and the nozzle height along the z-axis. Successive layers are deposited by incrementing the nozzle height and filaments are in suspension on the previous layer with a spanning distance L_1.

1. Introduction

Interactions with micro and nanochemical or biological entities have been improved with the recent advancements in microfluidic, microelectronic and microelectromechanic devices [1, 2, 3, 4]. For example, microelectronic devices are technically able to detect or measure adhesion and proliferation of specific pathogenic biomolecules [3, 4]. These advancements imply the use of new fabrication processes capable of dealing with more complex structures like the Direct-Write Method (DWM) which corresponds to processes that employ a deposition nozzle to extrude or deposite materials and a translation stage to create a controlled pattern on substrates or devices [5]. Robotic deposition is one of the DWM processes adapted for the deposition of various solid and soft materials in a two-dimensional (2D) pattern or a three-dimensional (3D) scaffold [6]. This scaffold is the first step of the fabrication process for micro-devices such as microfluidic mixers, drugs delivery systems [7], micro fuel cells [8] and heat exchangers for cooling system [9].

Figure 1 shows a 3D scaffold fabrication with a viscoelastic ink using robotic deposition process [10]. First, a patterned layer is deposited on a substrate by moving a x-y platform with adjusted extrusion nozzle height, diameter and deposition pressure. Then, extrusion nozzle height is incremented along the z-axis and successive layers are deposited until the desired scaffold is obtained. Each layer is composed of ink filaments supported by the previous layer with a defined spanning distance L_1 and filaments

present a diameter closed to the inner diameter of the extrusion nozzle.

The fabrication of 3D scaffolds can be time-consuming, depending on the final structure complexity ($\sim$ 78 minutes for a 104 layers scaffold consisted of a simple cubic lattice of 20 mm $\times$ 20 mm $\times$ 20 mm [10]). It is therefore of paramount importance that inks are mechanically adapted to minimize 3D scaffolds alterations as a function of time. Rheological studies led to the improvement of the inks viscoelastic properties [11, 12]. They are unable, however, to predict ink filament behaviour in scaffolds since they do not take into account the fact that inks are extruded under a filament shape and that the ink structure may be reorganized in the nozzle during extrusion [12]. Observations of mid-span time deflection of spanning filaments have allowed the definition of the minimum ink shear elastic modulus value allowed for limiting filament deflection in scaffolds [13]. Observations have also led to the development of a structural model for the time dependent deformation of a spanning ink filament simply supported at its extremities and under its own weight [11]. Similarly, filament mid-span time deflection observations are limited and can only be defined for a constant load corresponding to the filament spanning weight. In this paper, we present a tensile machine especially developed to characterize the mechanical behaviour of spanning ink filaments as those robotically deposited in scaffolds. This machine allows imposing various load levels as well as different strain rates. We also propose a data reduction procedure for obtaining the parameters of a linearly viscoelastic constitutive theory that best fit experimental data obtained from tensile tests.

2. Material, experimental method and data reduction procedure

2.1. Material

The organic ink is a mixture obtained by melting ($\sim$ 80 °C) and mixing ($\sim$ 20 minutes by magnetic stirring) petroleum jelly (*USP grade Vaseline®, Leverpond's Inc., Toronto, ON*) with a defined amount of microcrystalline wax (*SP18, Strahl & Pitsch Inc., West Babylon, NY*). At the end of the mixing period, the ink is poured in a syringe and immerged in cold water to avoid phases separation [12]. Microcrystalline wax content is typically between 10 to 40 weight percent (wt.-%) of the ink to allow the deposition of a 3D scaffold [10, 12].

2.2. Experimental Method

The tensile machine is represented in Figure 2 and is used to measure the mechanical properties of a robotically deposited ink filament spanning between a mobile and a fixed support. The mobile support is attached to four thin beams (*a* - *d*) clamped near their extremities in a machine frame. The frame is held by a MAX341 nano-positioning stage (*Thorlabs Inc., Newton, NJ*) able to manage 3-axis displacements with a 20 nm resolution using stepper motors and an APT Modular Rack controller (*Thorlabs Inc.,*

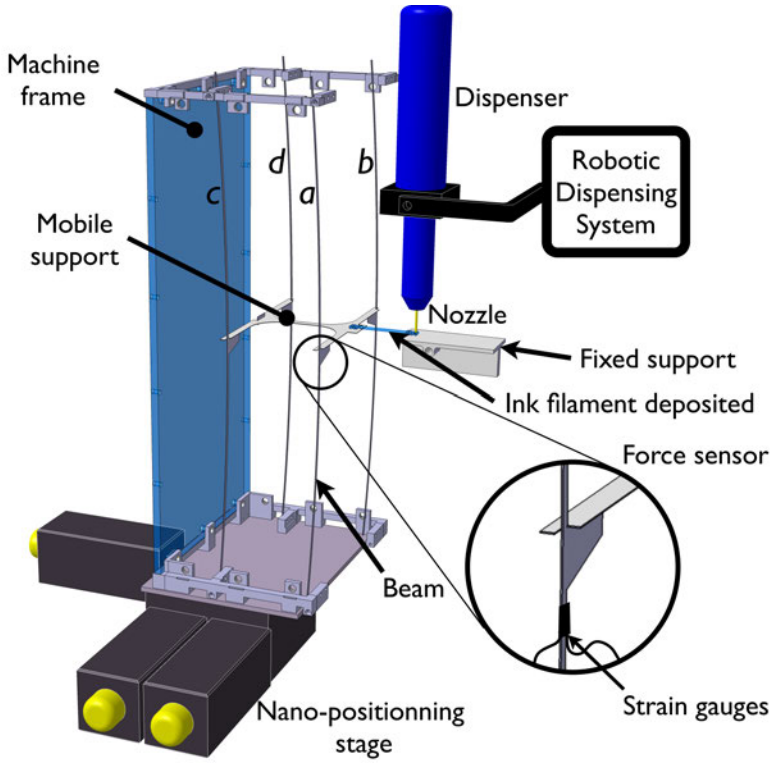

Figure 2. Schematic representation of the tensile machine used to measure the mechanical properties of a robotically deposited ink filament spanning between a mobile and a fixed support. The mobile support lays on four beams (*a*-*d*) clamped to the machine frame, held by a nano-positionning stage. Strain gauges placed on both sides of beams *a* and *b* are used to create a force sensor.

Newton, NJ). A 2 inch LT3 3-axis Travel Translation Stage (*Thorlabs Inc., Newton, NJ*) (not shown) is used to manually adjust the position of the fixed support (displacement resolution ~ 7 μm along the three axes) in order to keep both supports top surfaces aligned and to set the desired distance between them, called spanning distance L_0. Two strain gauges EP-XX-031DE-120 (*Vishay Intertechnology Inc., Malvern, PA*) placed on both sides of the beams *a* and *b* near their middle and oriented along the beams longitudinal axes are used to create a force sensor. After a calibration procedure, the measured longitudinal strains of beams *a* and *b* can be related to the applied force on the mobile support. For each beam (*a* and *b*), strain gauges are linked together to a Wheatstone half-bridge of a NI SC-2043-SG chipset (*National Instruments, Austin, TX*) connected to a NI PCI-6221 data acquisition card (*National Instruments, Austin, TX*). The measurements are then filtered using an exponential moving average, monitored and saved with a LabView program (*National Instruments, Austin, TX*). Exponential moving average is a common technique for filtering measurements obtained with sensors and is calculated, here, with a set of data acquired during 0.5 s. An ink filament can be extruded and deposited between these two supports using a I&J2200-4 Robotic Dispensing System (*I&J Fisnar Inc., Fair Lawn, NJ*), an Ultimus 2400 pressure regulator (*EFD Inc., Westlake, OH*) and a HP7x air powered dispenser (*EFD Inc., Westlake,*

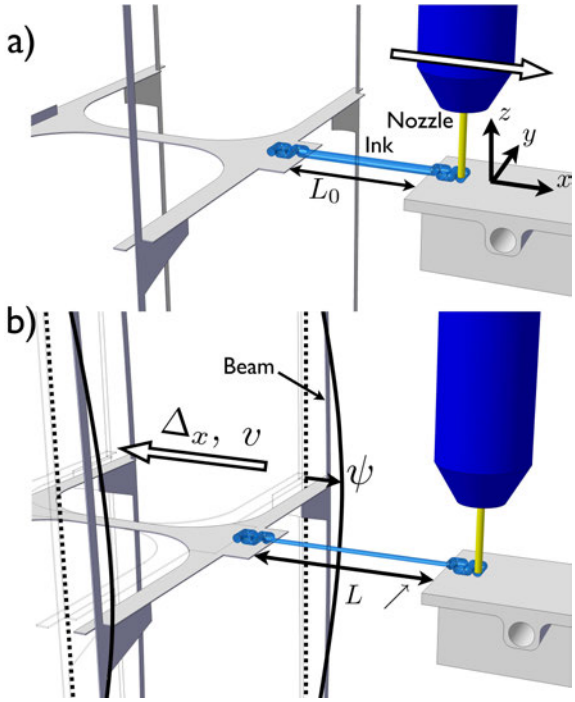

Figure 3. Schematic representation of a) the ink filament deposition along the x-axis between the two supports with a defined spanning distance L_0 and b) the ink filament tension along the x-axis due to the mobile support displacement Δ_x and the velocity v. The mobile support displacement increases the spanning distance L and induces ink filament inner forces due to its rigidity, which tends to displace the mobile support from ψ and to deform the four beams.

OH). The air powered dispenser contains a syringe filled with ink and, coupled with a general purpose micro-nozzle (*EFD Inc., Westlake, OH*), allows the deposition of ink filament in suspension between the two supports. Finally, the tensile machine is placed in a room at constant temperature near 21.5 °C.

Figure 3 shows the two main steps of the tensile test procedure. In the first step (Figure 3.a), an ink filament is extruded and deposited along the x-axis from the mobile support to the fixed support with a defined spanning distance L_0. The extrusion pressure and deposition velocity must be appropriate to connect a spanning filament to the two supports. Contacts between supports and ink filament have been checked to ensure that they present enough friction to avoid ink slipping using a digital video camera Evolution VF FAST Color 12-bit (*Media Cybernetics, Bethesda, MD*) with a resolution near 15 μm per pixel. In a second step (Figure 3.b), few seconds after the deposition of the filament, the nano-positionning stage is used to move the mobile support of Δ_x along the x-axis at the desired velocity v. By moving the mobile support, the spanning distance L increases and the ink filament is stretched. The induced force F due to ink filament tension tends to displace the mobile support of ψ along the x-axis and to deform the four thin beams. Therefore, induced force F during ink filament tensile test

can be deducted using the calibrated strain gauges measurements.

During the calibration procedure, different masses were successively applied on the mobile support using a pulley system. The gauge measurements demonstrated a linear response as a function of the applied force F_{applied} with a resolution of approximately 20 μN according to the ASTM E4-03 Standard and a maximum load capacity near 1 N. It was also demonstrated that the force sensor presents a response time near 1 s and an percent error equal to 3 % for an approximately applied force F_{applied} equal to 4 $\times 10^{-3}$ N.

2.3. Data reduction procedure

The data reduction procedure is based on a least square fit method between the experimental induced stress σ and the theoretical induced stress $\tilde{\sigma}$ for a linearly viscoelastic ink filament being stretched. σ is equal to $4F/\pi d^2$ where d is the filament diameter adjusted from its initial value $d_{\text{init.}}$ ($\varepsilon = 0$ %) as a function of the applied strain ε and the ink filament Poisson's ratio ν ($d = d_{\text{init.}}(1-\nu\varepsilon)$). For all measurements, ν is assumed to be constant and equal to 0.5 [11]. The initial ink filament mean diameter, $d_{\text{init.}}$, is measured at different positions along the spanning distance using a SZ61 stereomicroscope (*Olympus, Tokyo, Japan*) with a magnification of 3X and the Evolution VF FAST camera.

For a one-dimensional (1D) linearly viscoelastic material, the theoretical induced stress can be expressed as a function of the strain history by :

$$\tilde{\sigma}(t) = \int_0^t C(t-\theta)\ \frac{\mathrm{d}\varepsilon}{\mathrm{d}\theta}\mathrm{d}\theta \tag{1}$$

where $C(t)$ and ε represent the relaxation modulus and the applied strain, respectively. The relaxation modulus $C(t)$ is expressed as

$$C(t) = C' + \sum_{i=1}^{n} C_i \exp[-t/\lambda_i] \tag{2}$$

where C', C_i and $\lambda_i \geq 0$ for thermodynamic stability [14]. C' represents the fully relaxed modulus (i.e., for $t \to \infty$). The C_i and λ_i define the relaxation modes and n represents the number of relaxation modes. The instantaneous modulus (i.e., for $t \to 0$) is given by $C' + \sum_{i=1}^{n} C_i$. In the case of a tensile test conducted at a constant strain rate $\dot{\varepsilon}_0$, $\tilde{\sigma}$ is given by :

$$\tilde{\sigma}(t) = C' t\dot{\varepsilon}_0 + \dot{\varepsilon}_0 \sum_{i=1}^{n} \lambda_i C_i \Big(1 - \exp[-t/\lambda_i]\Big) \tag{3}$$

Then, if the strain is held constant after t_0 (i.e., a relaxation period), according to Boltzmann's superposition principle, $\tilde{\sigma}$ is given by :

$$\tilde{\sigma}(t) = C' t_0 \dot{\varepsilon}_0 + \dot{\varepsilon}_0 \sum_{i=1}^{n} \lambda_i C_i \Big(\exp[-(t-t_0)/\lambda_i] - \exp[-t/\lambda_i] \Big) \tag{4}$$

for $t \geq t_0$.

The least square problem used for obtaining C', C_i and λ_i is defined as [15, 16] :

$$\inf_{C', C_i \geq 0} R^2 = \inf \sum_{j=1}^{m} \alpha_j \Big[\sigma(t_j) - \tilde{\sigma}(t_j) \Big]^2 \tag{5}$$

where R^2, m and α_j are the residual value, the number of experimental data points and the weighting factors for each square value $[\sigma(t_j) - \tilde{\sigma}(t_j)]^2$, respectively. In the first step, the data reduction procedure is executed by fixing n and the λ_i a priori. Typically $n = 10$ was used and the λ_i were distributed on a log scale. In the second step, Equation (5) is solved and the C_i identified values that are much smaller than the others are removed. New λ_i are introduced around the remaining λ_i corresponding to the non-negligeable C_i. In the third step, Equation (5) is executed anew and the whole procedure is repeated until R^2 does not vary significantly. At the end, constitutive theory parameters C' and $\{C_i, \lambda_i\}$ are obtained. α_j can be adjusted when solving Equation (5) for several responses simultaneously, for which the number of data points might not be equal. This is detailed in Section 3.5 . The data reduction procedure is programmed and executed with the Global Optimization Toolbox of Maple 12 Software (*Maplesoft, Waterloo, ON*) and the algorithm employed is a local search.

3. Results and Discussions

Ink filament response to tensile test is measured for different strain rates ($\dot{\varepsilon}_0 = v \ / \ L_0$), microcrystalline wax amounts and extrusion nozzle inner diameters. The response is also measured for a tensile test with a defined strain rate $\dot{\varepsilon}_0$, followed by a relaxation test at $t = t_0$ with a constant strain $\varepsilon_1 = \dot{\varepsilon_0} \ t_0$.

At least 6 repetitions were conducted on different ink filaments for each parameters combination and each repetition respected the ink filament rupture requirements defined in the ASTM Standard C1557-03$^{\mathrm{E1}}$. The 95 % confidence intervals on the mean value are given for most of the measurements and only induced stress responses mean values are represented. The results are given for the interval $t \in [0, t_{\mathrm{f}}]$, where $t = 0$ and $t = t_{\mathrm{f}}$ correspond to the beginning of the tensile test and to the average ink filament rupture (characterized by the beginning of a decreasing slope of the induced stress response as a function of time). For the tension-relaxation test, measurements are stopped when acquired signals reach a stabilized value.

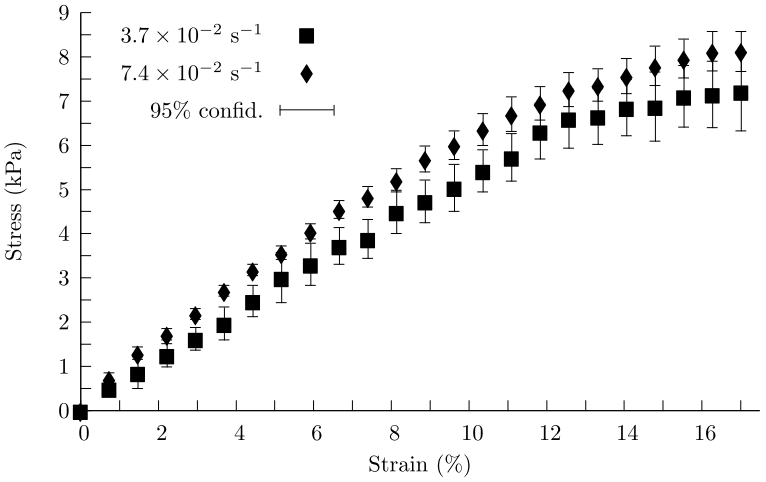

Figure 4. Evolution of the ink filament induced stress response as a function of applied strain during tensile tests conducted with two different strain rates, $\dot{\varepsilon}_0 = 3.7 \times 10^{-2}$ s^{-1} and 7.4 x 10^{-2} s^{-1} on 40 wt.-% ink filaments extruded with a 0.84 mm nozzle.

For all experiments, $L_0 = 10.67$ mm and tensile tests are mostly applied with $\dot{\varepsilon}_0 = 3.7 \times 10^{-2}$ s^{-1}, which is a compromise between too low strain rates implying measured induced force F in the same order of magnitude than the force sensor resolution in the time interval $t \in [0, t_f]$ and too important strain rates leading to ink filaments premature failures.

3.1. Ink filament response as a function of applied strain rate $\dot{\varepsilon}_0$

Figure 4 shows the induced stress response σ as a function of the applied strain ε during tensile tests conducted on 40 wt.-% ink filaments extruded with a 0.84 mm nozzle for $\dot{\varepsilon}_0 = 3.7 \times 10^{-2}$ s^{-1} ($v = 0.4$ mm.s^{-1}) and 7.4×10^{-2} s^{-1} ($v = 0.8$ mm.s^{-1}). Ruptures occur near $\varepsilon = 16.5$ % for both strain rates and the material appears to be stiffer as the strain rate is increased, suggesting that ink filaments are viscoelastic.

3.2. Ink filament response as a function of the microcrystalline wax amount

Figure 5 shows the induced stress response σ as a function of time obtained during tensile tests with $\dot{\varepsilon}_0 = 3.7 \times 10^{-2}$ s^{-1} conducted on ink filaments with different amounts of microcrystalline wax (10, 20, 30 and 40 wt.-%) and extruded with a 0.84 mm nozzle.

The induced stress response tends to increase with the amount of microcrystalline wax and the response in the case of the 20, 30 and 40 wt.-% ink filaments is 200 % or 300 % the value of the response of the 10 wt.-% ink filament. 20 and 30 wt.-% ink filament responses are similar and their 95 % confidence intervals overlap for $t <$ 3 s. Although the 20 wt.-% ink filament presents an instantaneous modulus higher than the 30 wt.-% ink filament for the same reason, instantaneous elastic modulus, defined as $E(t) = \sigma(t)/\varepsilon(t)$ with t near 0^+, tends to increase with the microcrystalline

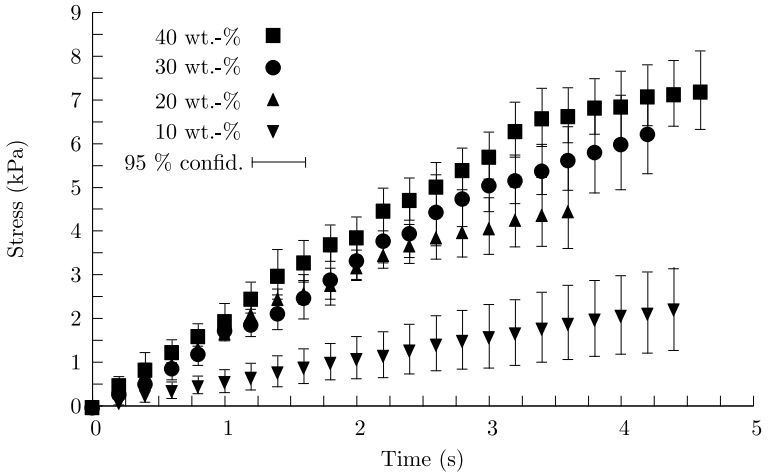

Figure 5. Evolution of the induced stress response as a function of time during tensile tests with $\dot{\varepsilon}_0 = 3.7 \times 10^{-2}$ s^{-1} conducted on ink filaments with four different amounts of microcrystalline wax : 10, 20, 30 and 40 wt.-%, and extruded with a 0.84 mm nozzle.

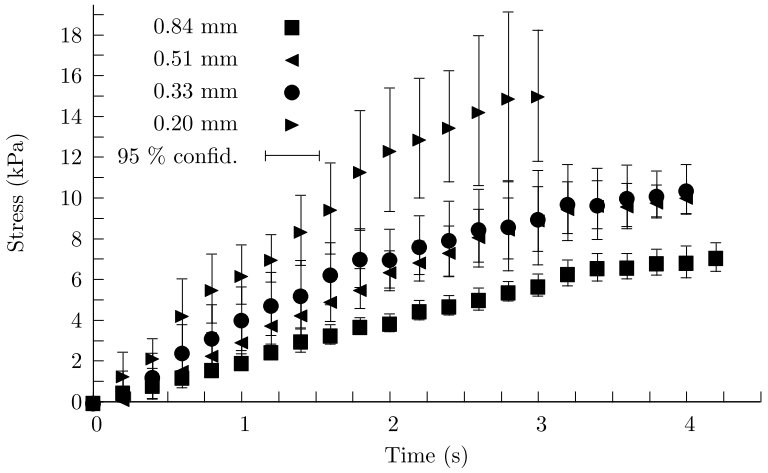

Figure 6. Evolution of the 40 wt.-% ink filament induced stress response as a function of time during tensile tests with $\dot{\varepsilon}_0 = 3.7 \times 10^{-2}$ s^{-1} conducted on filaments extruded with four different nozzle inner diameters : 0.84, 0.51, 0.33 and 0.20 mm.

wax content as shown in previous rheological studies [10, 12]. Instantaneous relaxation moduli are approximately equal to 16, 44, 41 and 53 kPa for the 10, 20, 30 and 40 wt.-% ink filaments. Finally, the 20 wt.-% ink filament presents a rupture around 3.6 s ($\varepsilon \sim 13.3$ %) in comparison to the 10, 30 and 40 wt.-% ink filaments breaking between 3.9 ($\varepsilon \sim 14.5$ %) and 4.5 s ($\varepsilon \sim 16.7$ %), supposedly due to inaccurate deposition parameters interfering with the mechanical behaviour of the 20 wt.-% ink filament.

3.3. Ink filament response as a function of extrusion nozzle inner diameter

Figure 6 shows the induced stress response σ as a function of time obtained during tensile tests with $\dot{\varepsilon}_0 = 3.7 \times 10^{-2}$ s^{-1} conducted on 40 wt.-% ink filaments extruded with different nozzle inner diameters (0.84, 0.51, 0.33 and 0.20 mm).

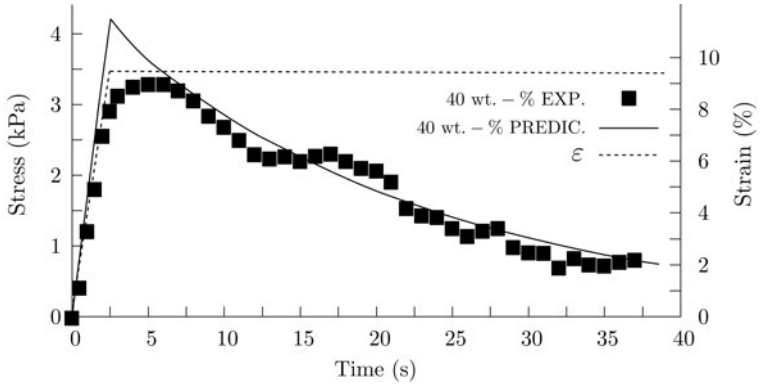

Figure 7. Evolution of the experimental induced stress response (40 wt.-% EXP.) of a 40 wt.-% ink filament extruded with a 0.84 mm nozzle as a function of time during a tensile ($\dot{\varepsilon}_0 = 3.7 \times 10^{-2}$ s^{-1}) and a relaxation ($\varepsilon_1 = 9.3$ %) test. The predicted response (40 wt.-% PREDIC.) based on the identified constitutive theory parameters is also shown.

The induced stress increases with the reduction of the nozzle inner diameter, although responses for the 0.33 and the 0.51 mm nozzles are similar. The response for the ink filament extruded with a 0.20 mm nozzle is nearly 200 % the responses with the 0.33 mm and 0.51 mm nozzles and nearly 300 % the response with the 0.84 mm nozzle. This increase may be explained by a microcrystalline alignment in the nozzle flow direction with a reduction of the nozzle inner diameter. This alignment might increase the ink filament stiffness along the extrusion (and testing) direction. In addition, the ink filament rupture occurs earlier with the diminution of the inner diameter of the nozzle. The rupture successively happens at $t = 3$ s ($\varepsilon = 11.1$ %) for the ink filament extruded with 0.20 mm nozzle, near 4 s ($\varepsilon = 14.8$ %) with the 0.51 mm and 0.33 mm nozzles and 4.5 s ($\varepsilon = 16.7$ %) in the case of the 0.84 mm nozzle. These successive ruptures confort the idea of a microcrystalline structure alignement phenomenon with a reduction of the nozzle inner diameter implying a decrease of the filament ductility. Finally, the reduction of the nozzle inner diameter leads to an increase of the 95 % confidence intervals. This might be due to the difficulty to align exactly ink filaments with the smaller diameters along the x-axis, which decreases the force measurements accuracy [17]. This also may be due to the measured force F for the filament extruded with the 0.20 mm nozzle which is only 20 % the force F measured in the case of the 0.84 mm nozzle and closer to the resolution of the force sensor.

3.4. Ink filament response to a tension-relaxation test

Figure 7 shows the induced stress response obtained during a tension-relaxation test conducted on a 40 wt.-% ink filament extruded with a 0.84 mm nozzle. The tensile test is conducted on the ink filament with $\dot{\varepsilon}_0 = 3.7 \times 10^{-2}$ s^{-1} and stops at $t_0 = 2.5$ s. The relaxation part consists of applying a constant strain ε_1 of 9.3 %. The ink

Table 1. Constitutive theory parameters C' and $\{C_i, \lambda_i\}$ identified for different ink filaments with distinct combination of microcrystalline wax amount and inner diameter of extrusion nozzle.

Microcrystalline wax (wt.-%)	Extrusion nozzle (mm)	C' (kPa)	i	C_i (kPa)	λ_i (s)
10	0.84	~ 0	1	16.19	13.0
20	0.84	~ 0	1	55.70	3.5
30	0.84	~ 0	1	49.19	11.8
40	0.84	~ 0	1	4.24	1.0
			2	46.05	21.0
40	0.51	~ 0	1	96.61	6.65
40	0.33	~ 0	1	132.41	2.85
40	0.20	~ 0	1	196.76	4.3

filament presents a quasi-linear induced stress response during the tension test and an exponential response with respect to time during the relaxation test. For $t > 32$ s, the stress response is fluctuating around 0.8 kPa and measurements are stopped at $t = 37.5$ s where the relaxation modulus i.e., $\sigma(37.5)/\varepsilon(37.5)$, is approximately equal to 9.3 kPa. The 95 % confidence intervals are not shown in order to keep a legible response.

For this particular strain history, the theoretical induced stress response in a viscoelastic material obeying Equation (2) should be maximum at $t = t_0$ and decreasing at t_0^+. However, the response reaches its maximum near $t = 5$ s and starts decreasing at $t = 6.5$ s. This ~ 3 s delayed response is supposed to be due to the response time of the sensor for measuring successively increasing and decreasing forces.

3.5. Identification of the constitutive theory parameters

Identification of the constitutive theory parameters C' and $\{C_i, \lambda_i\}$ is conducted for distinct ink filaments. Due to the previous mechanical observations, it is assumed here that a distinct ink filament corresponds to a combination of a certain microcrystalline wax content and a specific nozzle inner diameter. For each material, all experimental data has been used in the definition of R^2 from Equation (5). For example, in the case of the 40 wt.-% ink filament extruded with a 0.84 mm nozzle, experimental data of Figures 4, 5 and 7 (3.7×10^{-2} s^{-1}, 7.4×10^{-2} s^{-1} and 40 wt.-% EXP.) has been used to indentify the constitutive theory parameters.

Table 1 lists C' and $\{C_i, \lambda_i\}$ for distinct ink filaments. For any combination of microcrystalline wax amount and nozzle inner diameter, the ink filament exhibits a negligible stabilized response (C'). Further tensile and tension-relaxation tests over longer periods of time would be required for validating these values.

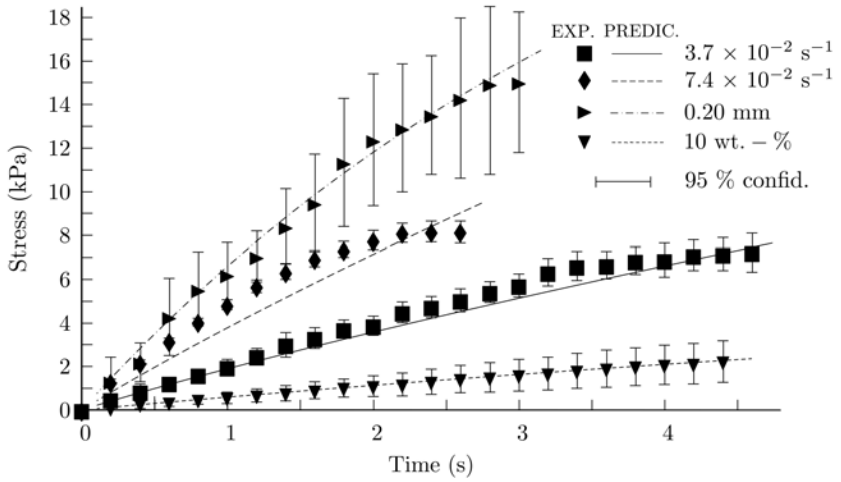

Figure 8. Evolution of the experimental induced stress response (EXP.) as a function of time during tensile tests conducted on the 10 and 40 wt.-% ink filaments (sections 3.2), the ink filament extruded with a 0.20 mm nozzle (section 3.3) and the ink filament stretched at $\dot{\varepsilon}_0 = 7.4 \times 10^{-2}$ s^{-1} (section 3.1). Predicted responses (PREDIC.) based on identified constitutive theory parameters are also shown.

In order to study the reliability of the identified parameters, Figure 8 shows, as an example, the experimental data (EXP.) measured for different materials i.e., 10 and 40 wt.-% ink filaments extruded with a 0.84 mm nozzle (sections 3.1 and 3.2) and the 40 wt.-% ink filament extruded with a 0.20 mm nozzle (section 3.3), with their corresponding predicted responses (PREDIC.) based on the identified constitutive theory parameters. The predicted responses are closed to the experimental data i.e., in the 95% confidence intervals, for the 10 wt.-% ink and the 0.20 mm nozzle ink filaments. Similar prediction results have been obtained for the other filaments, except for the 40 wt.-% and the 0.84 mm extrusion nozzle diameter.

For the 40 wt.-% ink filament extruded with a 0.84 mm extrusion nozzle, all available experimental data have been used. It was found, after trials and errors, that setting $\alpha_j = 4$ for $t \in [0, 2.5]$ seconds for the tension-relaxation test (and $\alpha_j = 1$ otherwise) led to model predictions fitting relatively well all the experimental data on Figures 7 and 8.

All these results show that a linearly viscoelastic constitutive theory might be a practical choice for modelling the mechanical behaviour of such ink filaments. Even though some discrepancies can be observed for the 40 wt.-% filament extruded with a 0.84 nozzle, the authors believe that the models obtained in this study could be useful for predicting scaffold behaviour and contributing to the optimization of DWM structures.

Subjecting the various filaments to different load histories (as was done for the 40 wt.-% filament extruded with a 0.84 nozzle) would allow determining the degree

of precision that can be expected from linearly viscoelastic constitutive theories for modelling the mechanical behaviour of ink filaments. The tension testing machine developed in this study is capable of generating a wide spectrum of uni-dimensionnal load histories and could be used to this end.

4. Conclusions

A custom-designed tensile machine has been used to characterize organic ink based on a mixture of petroleum jelly and a specific amount of microcrystalline wax when extruded and deposited as filaments. It has been shown that the ink filament response presents a strain rate dependence. We observed that increasing microcrystalline wax amount and decreasing the inner diameter nozzle lead to a stiffer ink filament. A tension-relaxation test conducted on a 40 wt.-% ink filament has shown that the material exhibits a viscoelastic behaviour. Constitutive theory parameters identification demonstrated that ink filaments behaviour is dominated by a delayed response and prediction responses based on these parameters are close to the experimental data. Further refinements are needed to improve the force sensor precision in order to maximize the duration of the tensile and tension-relaxation tests according to the ASTM C1557-03^{E1} Standard. These improvements will provide important information on the mechanical behaviour of ink filaments and their constitutive theory parameters under various loads which may find interest in being implemented in finite elements programs to simulate not only ink filaments in suspension but also scaffolds. We foresee that a similar approach could be applied for other ink materials such polyelectrolytes and nanocomposites.

Acknowledgments

The authors wish to acknowledge financial support from Natural Sciences and Engineering Research Council of Canada (NSERC).

References

[1] N. Bao, J. Wang, and C. Lu. Recent advances in electric analysis of cells in microfluidic systems. *Journal of Analytical and Bioanalitycal Chemistry*, 391(3):933 – 942, 2008.

[2] T. A. Franke and A. Wixforth. Microfluidics for miniaturized laboratories on a chip. *ChemPhysChem*, 9(15):2140 – 2156, 2008.

[3] A. Balasubramanian, B. Bhuva, R. Mernaugh, and F. R. Haselton. Si-based sensor for virus detection. *Sensors Journal*, 5(3):340 – 344, 2005.

[4] S. Bangalore Prakash and P. Abshire. Tracking cancer cell proliferation on a cmos capacitance sensor chip. *Biosensors & Bioelectronics*, 23(10):1449 – 1457, 2008.

[5] J. A. Lewis. Direct ink writing of 3d functional materials. *Advanced functional materials*, 16(17):2193 – 2204, 2006.

[6] R. Narayan. Recent developments in rapid prototyping of biomaterials. *Biotechnology Journal*, 2(11):1340 – 1341, 2007.

[7] D. Therriault, S. White, and J. Lewis. Chaotic mixing in three-dimensional microvascular networks fabricated by direct-write assembly. *Nature Materials*, 2:265 – 271, 2003.

[8] M. Kuhn, T. Napporn, M. Meunier, S. Vengallatore, and D. Therriault. Direct-write microfabrication and electrochemical testing of single-chamber micro solid oxide fuel cells. *Journal of Micromechanics and Microengineering*, 18, 2008.

[9] R. Bey-Oueslati, D. Therriault, and S. Martel. Pcb-integrated heat exchangers for cooling electronics using microchannels fabricated with the direct-write method. *IEEE Transaction on Components and Packaging Technologies*, 31(4):869 – 874, 2008.

[10] D. Therriault, R. Shepherd, S. White, and J. Lewis. Fugitive inks for direct-write assembly of three-dimensional microvascular networks. *Advanced Materials*, 17:395 – 399, 2005.

[11] D. Therriault, S. White, and J. Lewis. Rheological and structural behavior of fugitive inks for direct-write assembly. *Applied Rheology*, 17(1):10112–1 – 10112–8, 2007.

[12] J. Bruneaux, D. Therriault, and M.-C. Heuzey. Micro-extrusion of organic ink for direct-write assembly. *Journal of Microengineering and Micromechanics*, 18:115020–1 – 115020–11, 2008.

[13] J. E. Smay, J. Cesarano III, and J. A. Lewis. Colloidal inks for directed assembly of 3-d periodic structures. *Langmuir*, 18(14):5429 – 5437, 2002.

[14] M. Lévesque, K. Derrien, D. Baptiste, and M. Gilchrist. On the development and parameter identication of schapery type constitutive theories. *Mechanics of Time-Dependent Materials*, 12(2):95 – 127, 2008.

[15] M. Lévesque, M. D. Gilchrist, N. Bouleau, K. Derrien, and D. Baptiste. On applying the numerical laplace-carson transform inversion to the homogenisation of randomly reinforced linear viscoelastic media. *Computational Mechanics*, 40(4):771 – 789, 2007.

[16] R.B. Barello and M. Lévesque. Comparison between the relaxation spectra obtained from homogenization models and finite elements simulation for the same composite. *International Journal of Solids and Structures*, 45:850 – 867, 2008.

[17] H. J. Lee, H. S. Choi, C. S. Han, N. K. Lee, G. A. Lee, and T. H. Choi. A precision alignment method of the micro tensile testing specimen using mechanical gripper. *Journal of Materials Processing Technology*, 187 - 188:241 – 244, 2007.